Measurements of Raman scattering in the middle ultraviolet band from persistent chemical warfare agents

Fredrik Kullander*[b], Lars Landström[a], Hampus Lundén[b], Salam Mohammed[a],
Göran Olofsson[a], Pär Wästerby[a]
[a]CBRN-Defense and Security, [b]Sensor and EW Systems
Swedish Defense Research Agency (FOI), SE-901 82 Umeå, Sweden

ABSTRACT

The very low Raman scattering cross section and the fluorescence background limit the measuring range of Raman based instruments operating in the visible or infrared band. We are exploring if laser excitation in the middle ultraviolet (UV) band between 200 and 300 nm is useful and advantageous for detection of persistent chemical warfare agents (CWA) on various kinds of surfaces. The UV Raman scattering from *tabun*, *mustard gas*, *VX* and relevant simulants in the form of liquid surface contaminations has been measured using a laboratory experimental setup with a short standoff distance around 1 meter. Droplets having a volume of 1 µl were irradiated with a tunable pulsed laser swept within the middle UV band. A general trend is that the signal strength moves through an optimum when the laser excitation wavelength is swept between 240 and 300 nm. The signal from *tabun* reaches a maximum around 265 nm, the signal from *mustard gas* around 275 nm. The Raman signal from *VX* is comparably weak. Raman imaging by the use of a narrow bandpass UV filter is also demonstrated.

Keywords: Ultraviolet, Raman, chemical warfare agent detection, surface contamination, cross-section, tabun, mustard gas, VX

1. INTRODUCTION

The present capability to detect persistent chemical warfare agents (CWA) in the form of droplets or stains contaminating various surfaces is very limited. There are few kinds of fielded instruments for this purpose and they usually suffer from two drawbacks; they are based on contact with the contamination or the vapor above it and it takes time to use them. There are yet no detection systems able to provide fast and reliable detection of CWA over large surface areas[1]. Raman scattering can give specific vibrational signatures from the contaminations of interest and it is possible to measure the radiation from a stand-off position with an optical receiver. Commercial instruments are already available. These will typically provide non-contact measurement e.g. by the use of fiber optic coupled probe, but their achievable range is limited to a few centimeters. Even if this range is advantageous in terms of contamination avoidance there is also a need for a longer standoff range of up to tens of meters or more to enable a faster overall detection procedure. Most Raman instruments operate with a laser excitation wavelength of 785 nm which is partly explained by the availability of good laser sources. But this choice is generally also motivated by reduced interfering fluorescence compared to shorter laser excitation wavelengths, spectral resolution and by the applicability of silicon CCD detectors compared to instruments based on longer laser excitation wavelengths. Fluorescence will typically be emitted in a broad band that cover the Raman lines and give rise to excessive shot noise, hence reduced detectability. The fluorescence strength will in general be stronger for shorter laser wavelength since many naturally occurring substances have their absorption bands from the visible and down to the UV bands. In the middle UV (MUV 200-300 nm), however, the Raman lines will start to appear spectrally separated from the fluorescence. UV laser excitation is also expected to give a comparably high Raman cross section due to the expected λ^{-4}-dependence and due to potential resonance enhancement near allowed electronic transitions of the molecules. Additionally a combination of Raman and fluorescence spectroscopy is possible since the same instrumentation can be used for both[2, 3]. UV Raman has been studied previously for the purpose of CWA detection and cross-sections have been measured and compared with theory[4, 5]. However, the lack of practical tunable laser sources has limited most studies to one or a few laser excitation wavelengths in the UV.

Our previous experiments[6] have shown that some of the most important persistent CWA's have unique Raman features detectable in the MUV. We have mostly been working with small droplets of real agents and simulants, in the range from

Chemical, Biological, Radiological, Nuclear, and Explosives (CBRNE) Sensing XV,
edited by Augustus W. Fountain III, Proc. of SPIE Vol. 9073, 90730C · © 2014 SPIE
CCC code: 0277-786X/14/$18 · doi: 10.1117/12.2049815

0.1 to 1 µl in volume[7] in simplified laboratory conditions. In this work we have only used 1 µl droplets, although detection of much smaller droplets will be possible. The strength and the main spectral features of the Raman scattering from the substances have been characterized in order to give a ground for estimation of the required performance parameters of an operational Raman based stand-off system.

A particular feature of value in this application would be the ability to spatially resolve the remote scene, i.e. imaging, with respect to the Raman information. A basic function would simply be to be able to find and localize potentially harmful stains in the scene. The discrimination from the surrounding background is also making it possible to increase the signal to noise ratio. This technique has already been extensively studied at FOI for the detection of explosives residues[8]. A system with a tunable bandpass filter operating in the visible has been developed and a 355 nm laser based system is currently under development. However, tunable filters for the MUV are not yet readily commercially available components. We show in this work that the tunable UV laser can be combined with a fixed narrow bandpass filter put in front of an imaging device to discern different chemicals.

2. MATERIALS & METHODS

The main experimental arrangement is shown to the left in Figure 1. The setup can be changed from a spectrometer configuration to a filtered imaging configuration as shown to the right. This general setup has been continuously improved during a few years. It is built up around a tunable pulsed UV laser (*NT342B* from *Ekspla*) and a spectrometer (*Shamrock SR-500i-B1* spectrograph with *DH720I-18F-03* ICCD from *Andor*). Here, the scattered Raman is collected essentially in the backward direction to within a solid angle of about 0.03 steradian using a 30 cm diameter spherical collector mirror with a focal length around 0.65 m about 1.4 m from the target. When configured as a spectrometer the collected radiation is focused directly into a round-to-slit fiber (48x50µm from *Andor*) that leads to the spectrograph. The spectral resolution obtained with this setup was 0.1 nm corresponding to ~20 cm^{-1} @ 210 nm and ~10 cm^{-1} @ 300 nm. Filters can be placed in the focused path in front of the fiber. In these tests, however, no filters where used in the spectrometer configuration. This is possible thanks to the low backscattered radiation level obtained from the pure sample droplets placed on clean silicon wafer surfaces and greatly simplifies the analysis of the data.

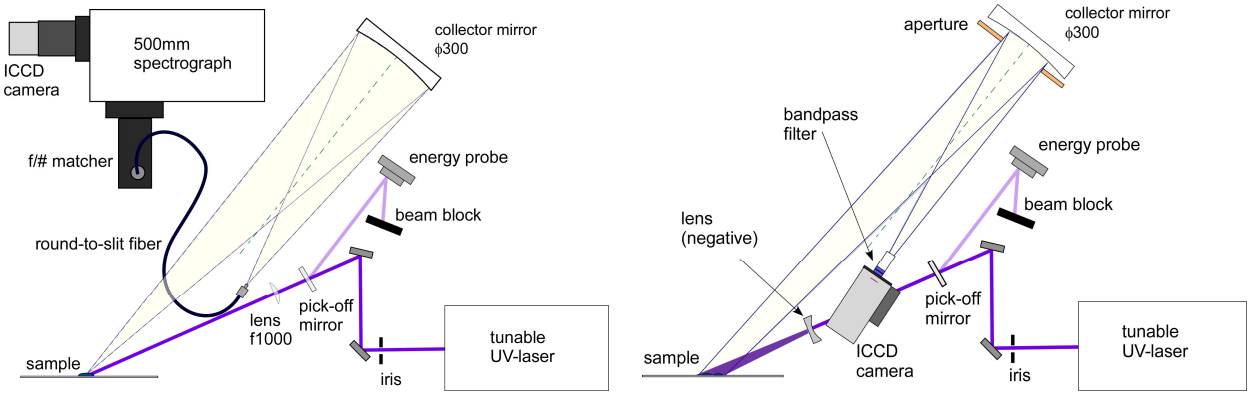

Figure 1. Experimental arrangement, to the left in a spectrometer configuration, to the right in imaging configuration.

A calibrated UV light source was employed to determine the efficiency of the spectrometer and its overall system transfer function, $H(\lambda)$. The light from the calibrated source was launched to an optical fiber (1 mm diameter) whose end was placed in the position of the sample to calibrate the spectrometer. The measured spectrometer transfer function $H(\lambda)=S(\lambda)/E_r(\lambda)$ is divided from the raw format detector data $S(\lambda)$ in units of counts to obtain an estimate of the energy of the radiation scattered into the solid angle of the receiver optics. Here, this received energy, denoted by $E_r(\lambda)$, represents the value measured in each spectral bin of the spectrometer per laser pulse[i]. Figure 2 shows the calibration fiber, the laser spot (saturated) on a piece of paper and a typical series of droplets applied to a silicon wafer surface.

[i] Integration over each Raman feature (typically one line) should be adopted to estimate its full energy.

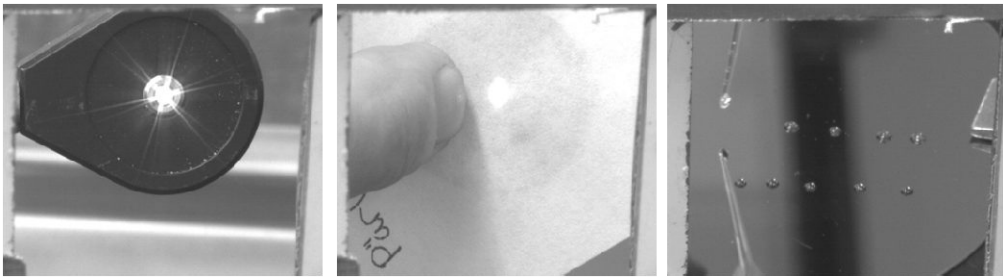

Figure 2. Calibration fiber, laser spot and application of 1µl droplets on silicon wafers.

The laser beam was focused using a 1 m focal length lens with the beam waist positioned behind the target distance. The incidence angle was about 45 degrees. The beam cross section profile at the target was roughly Gaussian with a beam diameter of 2.5 mm, see Figure 3. Excitation wavelengths from 211 nm to 300 nm were examined. The laser energy on the target was a function of wavelength and around 0.6 mJ at 211 nm and around 1.5 mJ at 300 nm. The energy fluence was thus ranging from 10 to 30 mJ/cm^2.

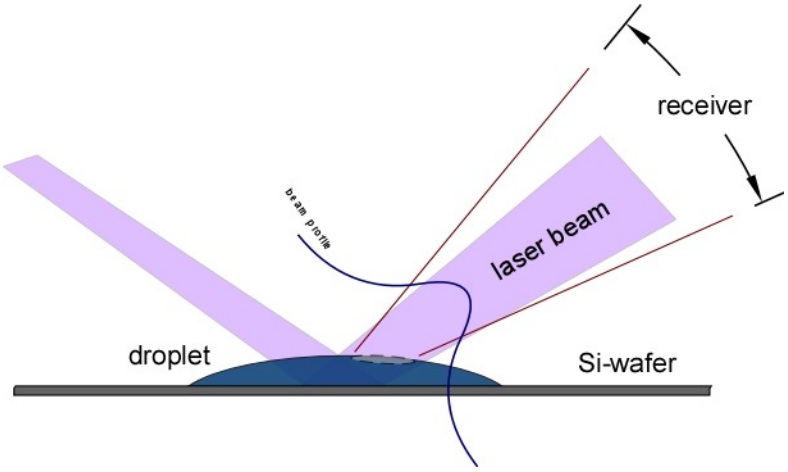

Figure 3. Geometry at target area.

In order to reduce the number of variables these spectral measurements were limited to 1 µl droplets applied on cleaned silicon wafer surfaces. Droplets of pure *Tabun* (GA), *mustard gas* (HD), *VX* and the simulants *triethyl-phosphonoacetate* (here denoted LT12), *tributyl-phosphate* (TBP) and *dimethyl-sulfoxide* (DMSO) were used. Additionally for the imaging tests data with *bis(4-chlorobutyl)-ether* (CBE) is shown[ii]. The ICCD gate was synchronized with the laser pulses and a 10 ns integration time was used for all data. The ICCD gain was set to its maximum value of 255 corresponding to ~650 counts/photoelectron except for the measurements on DMSO for which the gain had to be reduced to 180 corresponding to ~150 counts/photoelectron. The peak quantum efficiency of the ICCD is specified to 14%.

The measured collected energy of the Raman scattering is expected to be given approximately by

$$E_R(\lambda,\lambda_0) = n(\lambda,\lambda_0)\frac{E_0(\lambda_0)}{A_0}\frac{\partial\sigma_R(\lambda,\lambda_0)}{\partial\Omega}\Omega \qquad (1)$$

where n is the number of molecules effectively contributing to the Raman signal, E_0 is the excitation pulse energy, A_0 is the illuminated cross-section area (top-hat approximation) on the target, $\partial\sigma_R/\partial\Omega$ the differential Raman scattering

[ii] LT12= triethyl phosphonoacetate, CAS# 867-13-0, TBP= tributyl phosphate CAS# 126-73-8, DMSO= dimethyl sulfoxide CAS# 67-68-5, GA=tabun, CAS# 77-81-6, VX=VX, CAS# 50782-69-9, HD=distilled mustard, CAS# 505-60-2, CBE= bis(4-chlorobutyl) ether, CAS# 6334-96-9.

cross-section and Ω the solid angle extended by the collector mirror. The amount of molecules that contribute to the scattering is related to an effective illuminated depth of the target, *d*, by

$$n = NdA_n \tag{2}$$

where N is the number concentration and A_n is the effective cross section area visible to the receiver and illuminated by the laser beam. For a direct backscattering geometry the effective depth of illumination can be related to the absorption cross-section, σ_a and the sample thickness, D, by

$$d = \int_0^D e^{-(\sigma_a(\lambda_0)+\sigma_a(\lambda))Nz} dz \tag{3}$$

The absorption cross-section is typically becoming significant in the MUV band and the illumination depth can be expected to be dramatically reduced when the laser wavelength approaches absorption features of the molecules. This is evident for most of the tested chemicals here. UV absorbance data for these agents have been published previously[9] but we intend to make new absorbance measurements in the near future in order to be able to more accurately take the penetration depth functionality into account and possibly estimate the Raman cross-sections.

3. SPECTROMETER RESULTS

The way of measuring with droplets on pure silicon surfaces proved it viable to capture Raman spectrometer data without the use of a Rayleigh blocking filter. This is thanks to the relatively low elastic back scattering level with the wafer surface acting like a mirror. The non-ideal spectral leakage from the fundamental (Rayleigh) backscattering present in the spectrograph would otherwise cause saturation in the band of interest and prevent detection of the much weaker Raman scattering. Figure 4 shows an example of 'raw' data with a series of spectra from irradiation of LT12. A residual tail from the Rayleigh line in the form of an exponentially declining slope appears with a magnitude depending on the backscattering properties of the droplets. The spectral range of the spectrometer was continuously adjusted to get the laser wavelength just outside of the sensitive region of the ICCD. The Raman signal appears overlaid on this slope and can be faithfully reproduced as long as saturation is avoided. The main problem caused by this artifact is the excessive shot noise added to the signal but this was not limiting for these measurements.

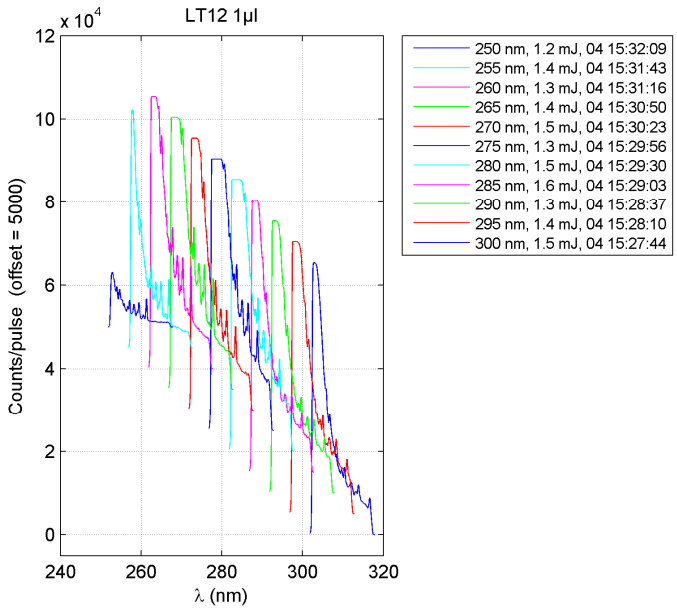

Figure 4. Raw data examples with spectra in the units of counts/pulse as a function of wavelength for excitation wavelength ranging from 250 nm to 300 nm.

The background, in the form of all broad features, was then removed [10] to obtain the estimated Raman signal.

Series of data with the laser excitation stepped down from 300 nm to 211 nm are presented below. The profile of the measured laser energy is also shown in the graphs. Care was taken to assure that the data at each laser excitation wavelength could be reproduced since some of the substances to a varying degree turned out to degrade as a function of the accumulated UV laser exposure. This was most evident for HD and LT12. The Raman signal as a function of laser excitation wavelength for LT12 is shown in Figure 5. The Raman strength for LT12 reaches a peak for a laser wavelength around 260 nm. The signal strength is then relatively rapidly falling with decreased laser wavelength. Kinetic series showed that the signal starts to degrade by the accumulated UV exposure already around 260 nm. This process gets faster and faster with shorter laser wavelength and it was not possible to reproduce the Raman data at longer laser excitation wavelength after exposure in the deeper UV, approximately below 250 nm. Fluorescence in the visible, not present from the unexposed droplet, was observed after the deep UV exposure.

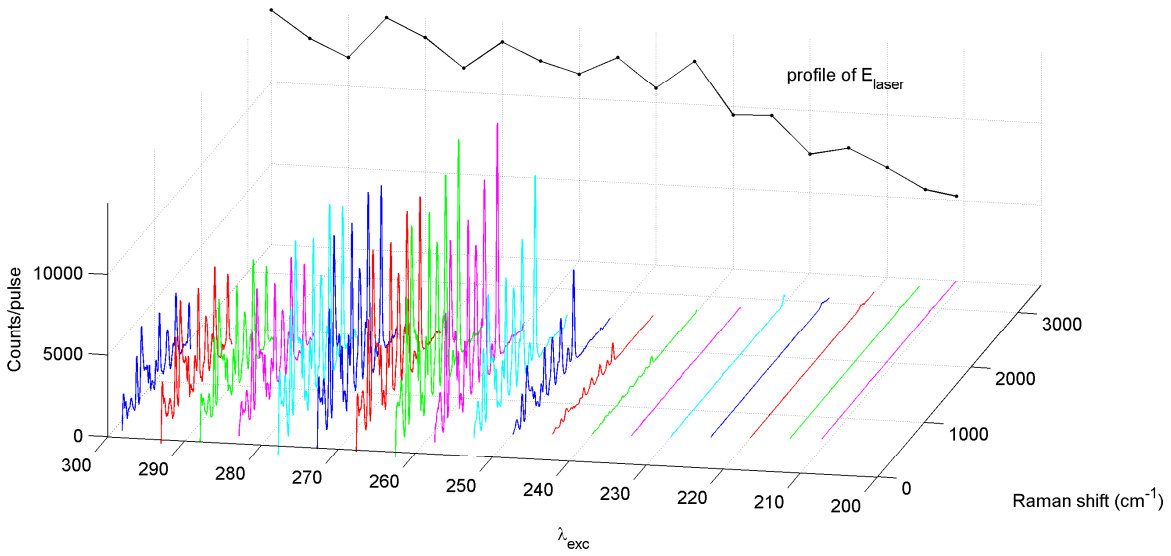

Figure 5. LT12, series of UV spectra, 300 nm down to 211 nm with 5 nm step. ICCD Gain set at 255, # of averaged pulses 100.

The Raman signal as a function of laser excitation wavelength for TBP is shown in Figure 6. The Raman signal from TBP is appreciable all the way down to 211 nm which can be explained by the relatively low UV absorbance for this substance. The commonly observed C-H band around 3000 cm^{-1} is visible in the deep UV spectra. There is no distinct optimum laser excitation wavelength and the signal strength is on the same order from about 270 nm down to 240 nm possibly even further down when the signal strength is compensated for the laser excitation energy. The signal from TBP is comparably stable and it is unclear whether or not this substance degrades by the UV exposure. The Raman signal as a function of laser excitation wavelength for DMSO is shown in Figure 7. The ICCD gain had to be set down for this substance due to a strong Rayleigh line tail. The Raman signal reaches a peak for a laser excitation wavelength around 270 nm and appears to drop as a result of increased absorption with decreasing laser excitation wavelength. Degradation of the Raman signal was seen as a result of the UV exposure but was not quantified in any detail.

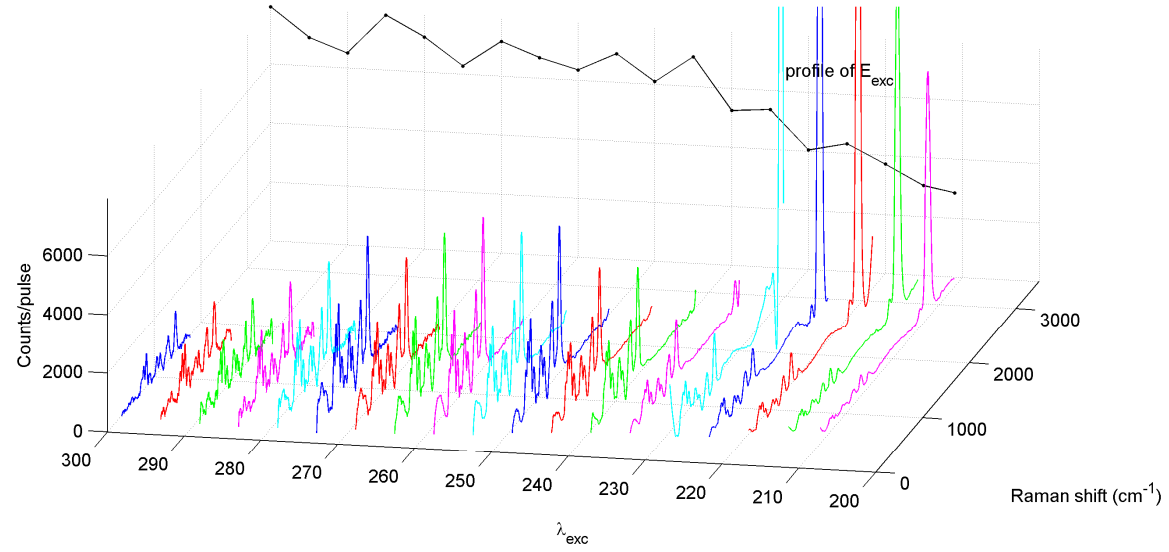

Figure 6. TBP, series of UV spectra, 300 nm down to 211 nm with 5 nm step. ICCD Gain set at 255, # of averaged pulses=100.

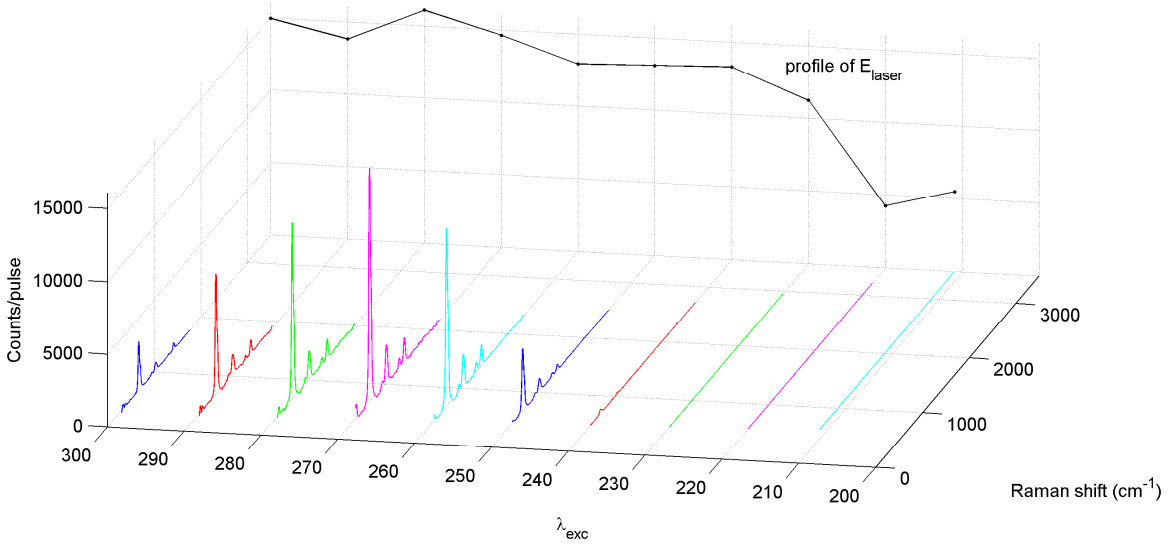

Figure 7. DMSO, 300 nm down to 211 nm with 10 nm step. ICCD Gain set at 180, # of averaged pulses=50.

The Raman signal as a function of laser excitation wavelength for VX is shown in Figure 8. The main observation for VX is unfortunately that the signal is comparably weak for all excitation wavelengths, almost two order of magnitudes weaker than for example GA and HD. A maximum may appear around 265 nm.

The Raman signal as a function of laser excitation wavelength for GA is shown in Figure 9. The signal maximizes at a laser excitation wavelength around 265 nm and is comparably strong. It exhibits its strongest peak, assigned to C-N

stretching vibrations [4], around 2200 cm^{-1}. The signal from GA is clearly degraded when exposed to the deeper UV radiation. Fluorescence in the visible, not present from the unexposed GA droplet, was observed after the deep UV exposure just like for LT12 droplets.

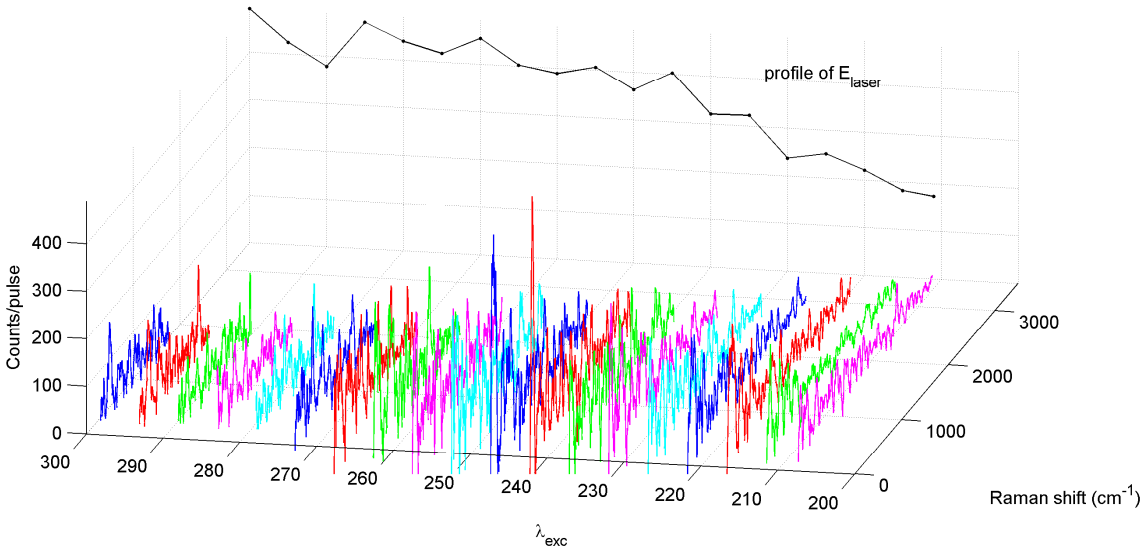

Figure 8. VX, series of UV spectra, 300 nm down to 211 nm with 5 nm step. ICCD Gain set at 255, # of averaged pulses=100.

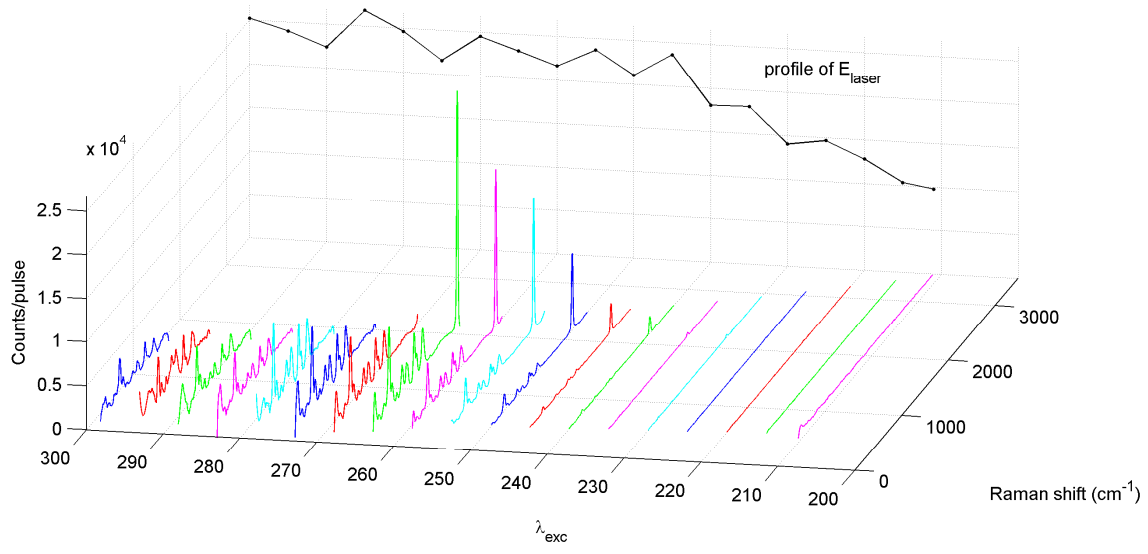

Figure 9. GA, series of UV spectra, 300 nm down to 211 nm with 5 nm step. ICCD Gain set at 255, # of averaged pulses=200.

The Raman signal as a function of laser excitation wavelength for HD is shown in Figure 10. The laser excitation wavelength dependence of the signal from HD as well as the spectrum is similar to its simulant DMSO. A peak Raman signal strength is reached around 270 nm with the strongest feature around 700 cm^{-1}. However, in difference from DMSO the Raman signal from HD is clearly decaying for laser excitation wavelengths below 275 nm. The decay rate increase rapidly with decreasing laser excitation wavelength. Fluorescence in the visible is also observed after repeated UV exposure. The number of averaged pulses was only 10 in this series due to the rapid extinction of the Raman signal caused by the exposure.

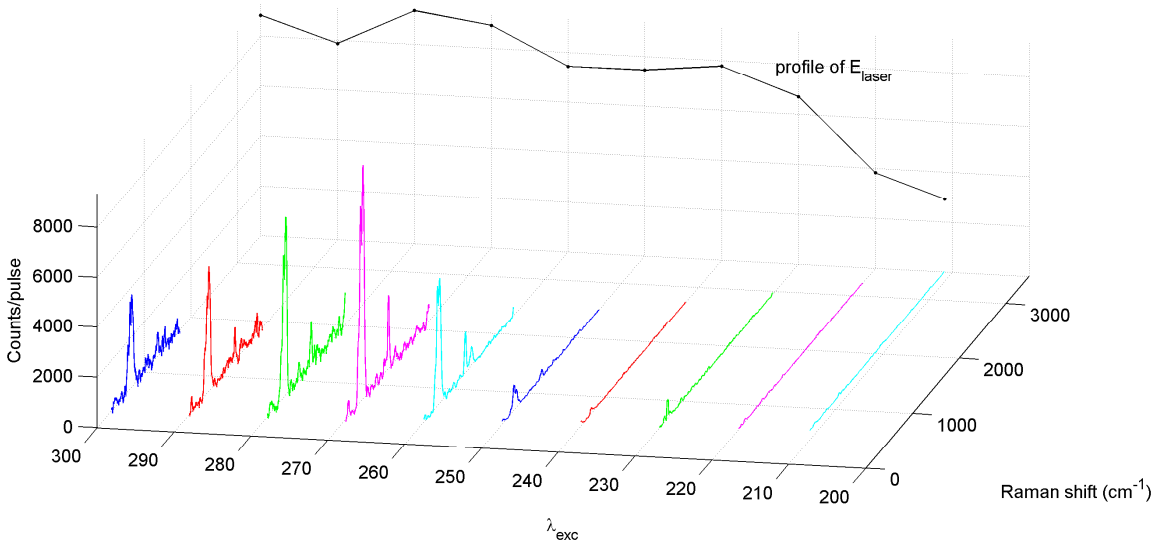

Figure 10. HD, series of UV spectra, 300 nm down to 211 nm with 10 nm step. ICCD Gain set at 255, # of averaged pulses=10.

Averaged spectra from irradiation at the laser excitation wavelengths where the signal was found to be strongest are shown in Figure 11. The expected shifts for N_2 and O_2, if visible, have been marked by colored lines. The signal strength reaches up to a level of 10^{-13} J/bin (~3 cm^{-1}/bin @ λ_{exc} =250-275nm) for all substances but VX. This level enables detection of the main spectral feature with a single laser pulse from this experimental setup. Averaging of 50-200 pulses, as was used here, is resulting in strong and noiseless Raman spectra. The Raman signal from VX required averaging from 5000 pulses and the peak from O_2 appears as the strongest in the spectrum. None of the other peaks and features can be faithfully associated to VX and may arise from the background. Further measurements are required to establish this spectrum but the signal strength is clearly relatively low.

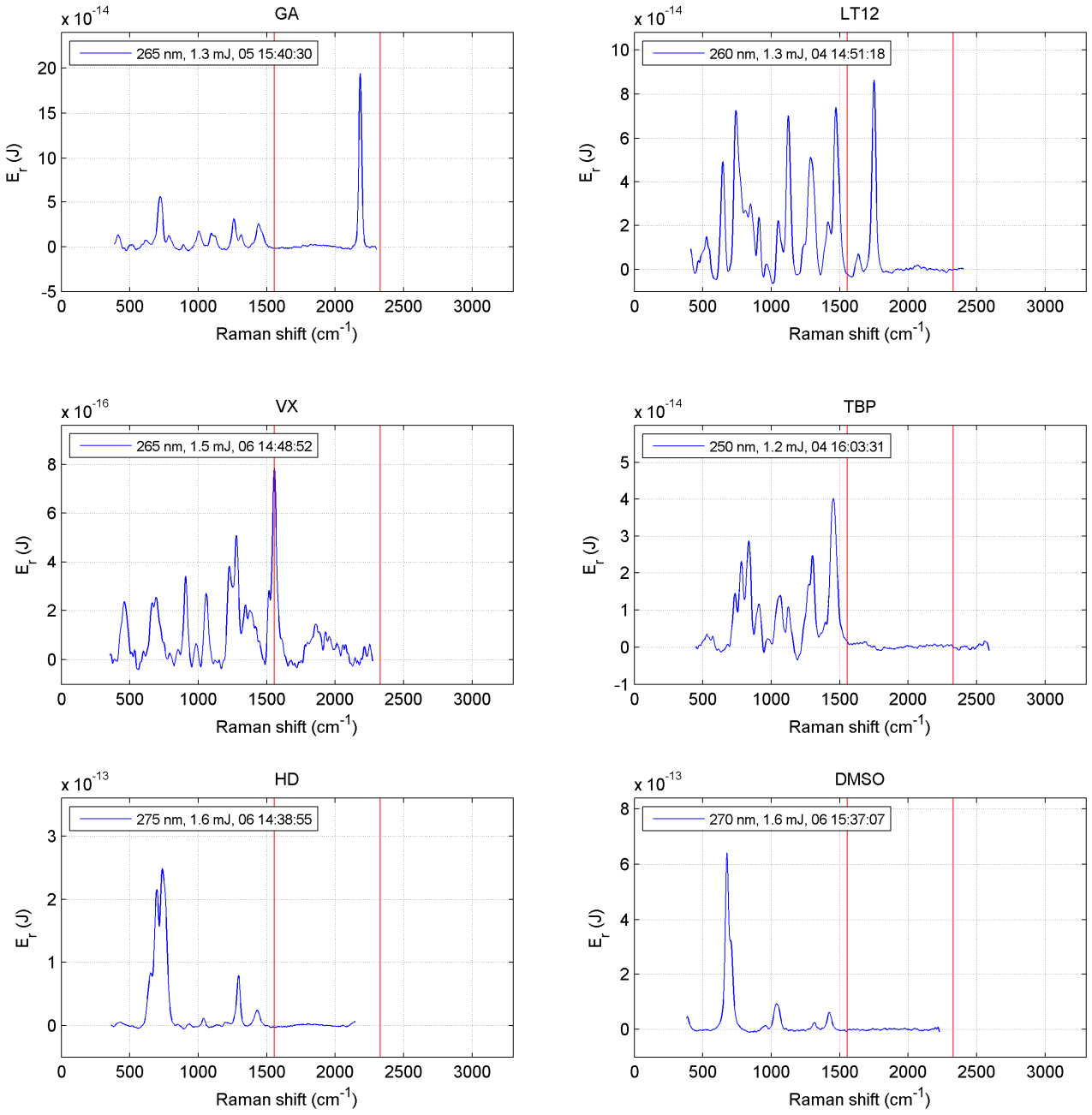

Figure 11. Spectra for each of the agents at the apparent optimum excitation wavelength. Averaging from several pulses was used, 50 to 200 pulses for all except for VX where an average from 5000 pulses is presented.

4. IMAGING RESULTS

Preliminary results from the imaging Raman spectroscopy setup have demonstrated the possibility of discriminating different CWA simulant droplets both against various backgrounds and against each other. Spectral images were created by stepping the excitation wavelength between 250 nm and 261 nm and monitor the signal through a bandpass filter centered at 265 nm. This resulted in a range of detected Raman shifts between ~700 cm^{-1} and ~2400 cm^{-1}. A combination

of fixed filters was used to achieve a 3 nm pass band corresponding to a wavenumber resolution of roughly 400 cm^{-1}. The field of view of the image was 40 mm times 10 mm, though the laser spot was limited to a radius of approximately 10 mm.

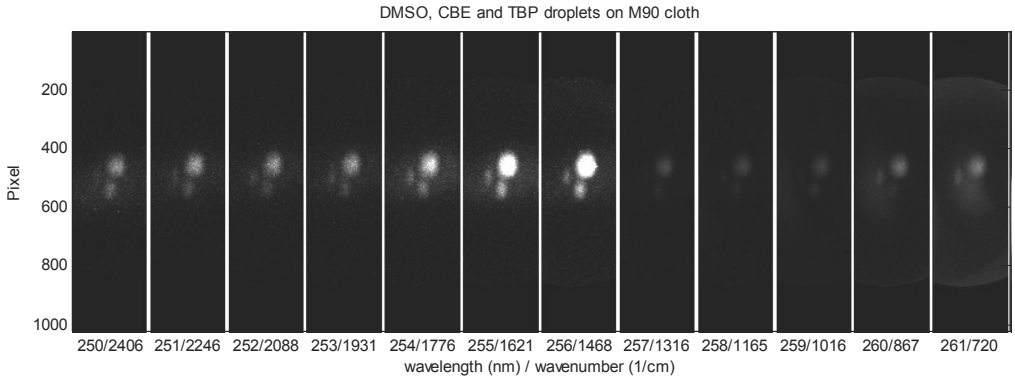

Figure 12. Three droplets of CWA simulants, the large spot to the right in each image is from CBE, the middle size spot at the bottom is from TBP, and the small left spot is from a DMSO droplet. The background was a piece of fabric from a Swedish military (M90) uniform.

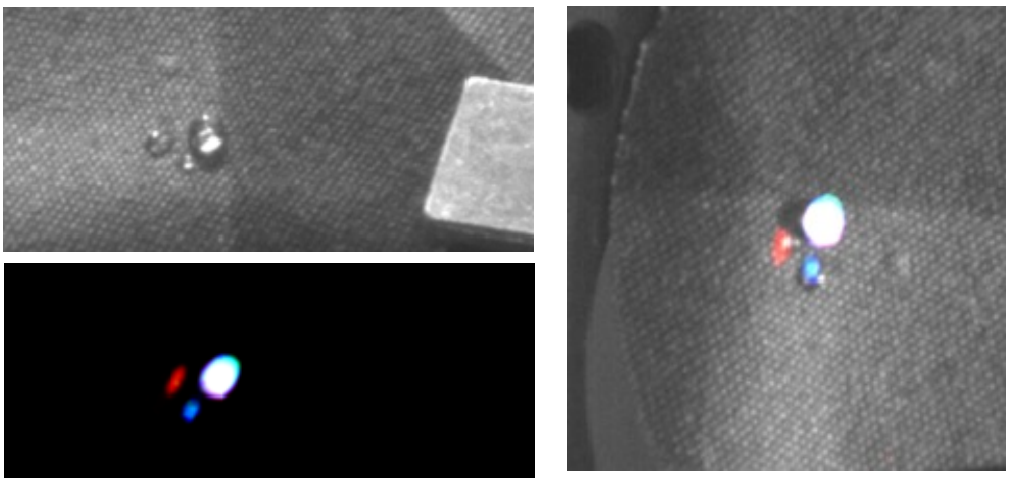

Figure 13. By digitally subtracting the background, strongly filtering the data and superimposing it color coded on a normal black-and-white image of the scene, it is possible to easily discriminate between the different droplets. The composite image to the right has been rotated and flipped to conform with the series displayed in Figure 12. The CBE droplet appears as white, DMSO as red and TBP as blue.

5. DISCUSSION AND CONCLUSIONS

The general trend with respect to the laser wavelength in the MUV band for these substances is that the Raman signal strength reaches a maximum in a band between 250 nm and 275 nm. A smooth increase is observed when the laser wavelength is adjusted down from 300 nm to the optimum and is steepest for HD and DMSO. These are also the ones with the strongest Raman signals. Absorption is then likely to come into play for shorter excitation laser wavelengths. The increased absorption reduces the effective penetration depth of the laser excitation into the targets.

The results apply for the quite simplified conditions in these experiments and in particular for droplets of this size and geometry. We have seen in other trials that the laser excitation optimum is shifted towards shorter wavelengths with thinner layers or smaller droplets, in agreement with the dependence expected from equation (3).

Resonance or pre-resonance enhancement in the form of a relatively distinct function of laser excitation wavelength as expected from preliminary simulations using density functional theory [11] is not observed in the experimental data. This possible enhancement may be completely offset by absorbance under the conditions of the experiment and it remains unclear if the effect can be utilized for this application.

The received energy levels according to Figure 11 have a relatively large uncertainty, in part caused by the aberrations of the optics. The uncertainty in terms of the absolute level is estimated to be about a factor of four. A known underestimation by a factor of two of the received energy from all of the illuminated cross section is due to the fact that the calibration was made with a 1 mm diameter optical fiber while the laser spot diameter was about 2.5 mm. Another uncertainty of great concern arises from the fact that the deep UV excitation tend to degrade the samples. This was carefully accounted for in these tests, e.g. by avoiding exposure by many laser pulses.

The level of uncertainty, however, is low enough to enable a ground for estimation of the required performance parameters of a potential operational Raman based stand-off system which was one underlying goal of this work.

6. ACKNOWLEDGEMENT

This work was funded by the Swedish Department of Defense, project number 440-A403914.

REFERENCES

[1] Fountain III, A. W., Guicheteau, J. A., Pearman, W. F., Chyba, T. H., and Christesen, S. D., "Long-range standoff detection of chemical, biological, and explosive hazards on surfaces," SPIE **7679**, 76790H (2010).
[2] Hug, W. F., Reid, R. D., Bhartia, R., and Lane, A. L., "Performance status of a small robot-mounted or hand-held, solar-blind, standoff chemical, biological, and explosives (CBE) sensor," SPIE **7304**, 73040Z (2009).
[3] Grun, J., Bowles, J., Gillis, D., Kunapareddy, P., Lunsford, R., Manka, C. K., Nikitin, S., and Wang, Z., "Tunable multi-wavelength resonance-Raman detection of bacteria and chemicals in complex environments," SPIE **7687**, 768706 (2010).
[4] Christesen, S. D., Jones, J. P., Lochner, J. M., and Hyre, A. M., "Ultraviolet Raman spectra and cross-sections of the G-series nerve agents," Applied Spectroscopy **62**(10), 1078-1083 (2008).
[5] Christesen, S. D., "Raman cross sections of chemical agents and simulants," Applied Spectroscopy **42**(2), 318-321 (1988).
[6] Kullander, F., Landström, L., Lundén, H., Mohammed, A., Olofsson, G., and Wästerby, P., "Development of Ultraviolet Raman scattering for standoff detection of chemical warfare agents," Proceedings of the *11th International Symposium on Protection against Chemical and Biological Warfare Agents*, Stockholm, 3-5 June (2013).
[7] Kullander, F., Landström, L., Lundén, H., Mohammed, A., Olofsson, G., and Wästerby, P., "Evaluation of technology for detection of CWA contamination - UV Raman spectroscopy of CWA droplets on silica surfaces," FOI MEMO 4235, FOI (2013).
[8] Östmark, H., Nordberg, M., and Carlsson, T. E., "Stand-off detection of explosives particles by multispectral imaging Raman spectroscopy," Applied Optics **50**(28), 5592-5599 (2011).
[9] Rewick, R. T., Schumacher, M. L., and Haynes, D. L., "UV absorption specta of chemical agents and simulants," Applied Spectroscopy **40**(2), 152-156 (1986).
[10] Mazet, V., Carteret, C., Brie, D., Idier, J., and Humbert, B., "Background removal from spectra by designing and minimising a non-quadratic cost function," Chemometrics and intelligent laboratory systems **76**(2), 121-133 (2005).
[11] Mohammed, A., Ågren, H., and Norman, P., "Time-dependent density functional theory for resonant properties: resonance enhanced Raman scattering from the complex electric-dipole polarizability," Physical Chemistry Chemical Physics **11**(22), 4539-4548 (2009).